

Disorder-Driven Exceptional Points and Concurrent Topological Phase Transitions in Non-Hermitian Lattices

Xiaoyu Cheng,¹ Tiantao Qu,² Yaqing Yang,¹ Lei Zhang,^{1,3,*} and Jun Chen^{2,3,†}

¹*State Key Laboratory of Quantum Optics Technologies and Devices,
Institute of Laser Spectroscopy, Shanxi University, Taiyuan 030006, China*

²*State Key Laboratory of Quantum Optics Technologies and Devices,
Institute of Theoretical Physics, Shanxi University, Taiyuan 030006, China*

³*Collaborative Innovation Center of Extreme Optics, Shanxi University, Taiyuan 030006, China*

Exceptional point (EP) and topological phase transition (TPT) in non-Hermitian systems have recently garnered significant attention owing to their fundamental importance and potential applications in sensing and topological devices. Beyond the EP induced by non-reciprocal hopping, we show that random disorder can also drive the valence and conduction bands across EPs, even twice in the non-Hermitian regime. Remarkably, a TPT can occur concurrently with an EP as disorder strength increases. These disorder-driven EPs and concurrent TPTs are well captured by effective medium theory. The analysis reveals that their emergence results from the interplay between disorder-induced energy level renormalization and non-reciprocal hopping-induced inter-level coupling, which fundamentally restructures the spectral properties of the system. The phase diagram in the parameter space of non-reciprocal hopping and disorder strength identifies robust EP lines. Interestingly, two EP lines can emerge from the TPT point in the Hermitian limit. As non-reciprocal hopping increases, these lines split, with one aligning the TPT, leading to distinct disorder-induced EPs. Our results uncover a robust, disorder-driven mechanism for generating EPs and concurrent TPTs, offering a new direction for exploring non-Hermitian topological matter.

Introduction.—Non-Hermitian systems, characterized by gain and loss or non-reciprocal hopping, have emerged as a fertile platform for exploring exotic physical phenomena, including exceptional point (EP) [1–7], PT symmetry breaking [8, 9], and non-Hermitian topology, etc [10–17]. In contrast to their Hermitian counterparts, non-Hermitian systems exhibit a complex interplay between spectral properties and symmetries, giving rise to phenomena such as the non-Hermitian skin effect [18–23] and topological phase transition (TPT) [22, 23]. These unique features have stimulated extensive interest in understanding the intricate relationship between symmetry and topology in non-Hermitian systems.

In reality, random disorder is inevitable and typically disrupts energy degeneracies. However, in certain cases, disorder can induce degeneracies. For instance, during disorder-driven TPT, energy degeneracies emerge at the transition point. It has been shown that a trivial phase can evolve into a topological nontrivial phase driven by disorder in both Hermitian and non-Hermitian systems [24–49]. Furthermore, the effect of disorder in Hermitian systems can be understood from the perspective of non-Hermitian self-energy. In this framework, disorder can give rise to the emergence of EPs or EP lines in momentum space [50, 51]. Nevertheless, the interplay between random disorder and EPs in non-Hermitian systems remains elusive. Several key questions arise: Can EP, a hallmark feature of non-Hermitian systems, be induced by random disorder? Since energy degeneracy happens in both EP and TPT, can disorder-induced EP coincide with TPT in non-Hermitian systems?

In this letter, we theoretically investigate the interplay between disorder, non-Hermitian and topology in a

lattice model. In the clean system, we find that the non-reciprocal coupling drives the valence and conduction bands through an EP, regardless of the system’s topology. Especially, non-reciprocal coupling can induce an EP accompanied by a concurrent TPT when the Hermitian system is initially topologically nontrivial. Upon introducing disorder into a topologically trivial non-Hermitian system, we find that as disorder strength increases, two EPs emerge, with their eigenvalues undergoing a real-complex-real transition. More significantly, random disorder drives the system from a trivial insulator to a topological insulator at the second EP, marking a concurrent TPT. We also observe a single EP accompanied by a TPT in another scenario, where the system transitions back to a topologically nontrivial phase due to disorder. Using effective medium theory, we explain the physical origins of the EPs and concurrent TPTs induced by disorder. Finally, from the phase diagram of non-reciprocal hopping and disorder strength, we identify EP lines, highlighting the robustness of EPs formation.

Non-Hermitian system.—To explore the interplay between disorder, non-Hermitian and topology, we begin with a generic tight-binding model on an atomic basis with three orbitals (s, p_x, p_y) per site [43, 44, 52, 53]. The Hamiltonian in real space is expressed as

$$\begin{aligned}
 H = & \sum_{i\alpha} \varepsilon_\alpha c_{i\alpha}^\dagger c_{i\alpha} + \sum_{\langle i\alpha, j\beta \in \text{right} \rangle} t_{\alpha, \beta}(\mathbf{r}_{ij}) e^{\kappa} c_{j\beta}^\dagger c_{i\alpha} \\
 & + \sum_{\langle i\alpha, j\beta \in \text{left} \rangle} t_{\alpha, \beta}(\mathbf{r}_{ij}) e^{-\kappa} c_{j\beta}^\dagger c_{i\alpha} \\
 & + i\lambda \sum_i \left(c_{ip_y}^\dagger \sigma_z c_{ip_x} - c_{ip_x}^\dagger \sigma_z c_{ip_y} \right),
 \end{aligned} \tag{1}$$

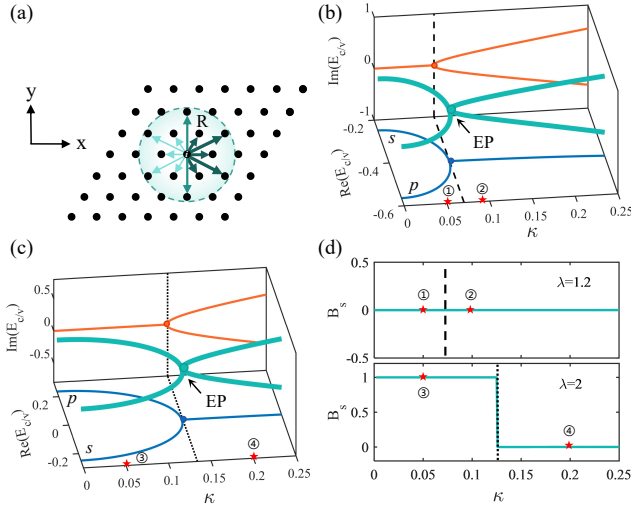


FIG. 1. (a) Schematic of a two-dimensional lattice structure. Arrows indicate the couplings between atom i and its neighboring atoms, with dark (light) green arrows representing hoppings to the right (left) of atom i . The cutoff radius is $R = 1.9a$, where a is the lattice constant. (b)-(c) Real and imaginary parts of the conduction (E_c) and valence (E_v) band energies as a function of non-reciprocal coupling strength κ when $\lambda = 1.2$ and 2 , respectively. The other parameters are $a = 1$, $\varepsilon_s = 1.8$, $\varepsilon_p = -6.5$, $V_{ss\sigma} = -0.256$, $V_{sp\sigma} = 0.576$, $V_{pp\sigma} = 1.152$, $V_{pp\pi} = 0.032$. (d) Spin Bott index B_s as function of κ , with the upper and lower panels shows corresponding to the results in (b) and (c), respectively. The system size is 50×50 with periodic boundary conditions.

where $c_{i\alpha}^\dagger = (c_{i\alpha,\uparrow}^\dagger, c_{i\alpha,\downarrow}^\dagger)$ represents the creation operator at site i with α denoting three orbitals. The ε_α describes the on-site energy of α orbital. The λ is the spin-orbit coupling strength, and σ_z is the Pauli matrix. The hopping integral $t_{\alpha,\beta}(\mathbf{r}_{ij})$ between different lattices is defined as [43, 44]:

$$t_{\alpha,\beta}(\mathbf{r}_{ij}) = \frac{\Theta(R - r_{ij})}{r_{ij}^2} \text{SK} [V_{\alpha\beta\delta}, \hat{\mathbf{r}}_{ij}], \quad (2)$$

where R is the cutoff radius, and $\Theta(R - r_{ij})$ is a step function. The function $\text{SK}[\cdot]$ represents Slater-Koster parametrization for three orbitals, where $V_{\alpha\beta\delta}$ are the bond parameters, and $\hat{\mathbf{r}}_{ij}$ denotes the unit direction vector [54]. To incorporate non-reciprocity, we introduce the non-reciprocal factor κ to the hopping terms. Taking atom i as the reference point, as illustrated in Fig. 1(a), we define hopping to the ‘‘right’’ ($x_j - x_i > 0$) within the cutoff radius to be weighted by e^κ , while hopping to the ‘‘left’’ ($x_j - x_i < 0$) is weighted by $e^{-\kappa}$.

We first investigate the effects of non-reciprocal hoppings on the eigenenergies and topological properties of the system under periodic boundary conditions. The Hermitian system can be either topologically trivial or nontrivial (exhibiting the quantum spin Hall effect), depending on the spin-orbit coupling strength λ [43, 44].

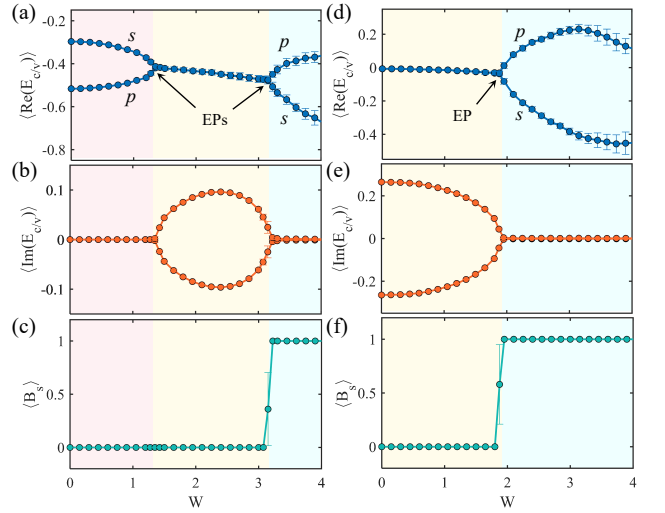


FIG. 2. (a)-(c) Disorder-averaged $\langle \text{Re}(E_{c/v}) \rangle$, $\langle \text{Im}(E_{c/v}) \rangle$ and $\langle B_s \rangle$ as functions of disorder strength W for $\kappa = 0.05$, $\lambda = 1.2$ respectively. (d)-(f) Disorder-averaged $\langle \text{Re}(E_{c/v}) \rangle$, $\langle \text{Im}(E_{c/v}) \rangle$ and $\langle B_s \rangle$ as functions of disorder strength W for $\kappa = 0.2$, $\lambda = 2$, respectively. Error bars represent the fluctuation in the disorder average. Each data point is averaged over 100 disorder realizations, with other parameters identical to those in Fig. 1.

In the topologically trivial (nontrivial) phase, the conduction (E_c) and valence (E_v) bands are dominated by s/p (p/s) orbitals, respectively. As shown in Fig. 1(b) and 1(c), regardless of the Hermitian system’s topological property, the real parts of E_c and E_v gradually coalesce as κ increases and become degenerate beyond a critical value. Simultaneously, the corresponding imaginary parts remain zero before transitioning into nonzero conjugate pairs beyond the critical point, marking the system’s passage through an EP. Notably, when the system is initially in a topologically nontrivial phase, non-reciprocal hopping induces a concurrent TPT at the EP, as evidenced by the sharp jump in the spin Bott index shown in the lower panel of Fig. 1(d). This transition is driven by the closing of the real part of the energy (topological) gap at the EP, rendering the system topologically trivial. In contrast, no TPT occurs when the system is initially topologically trivial, as shown in the upper panel of Fig. 1(d). Consequently, clean non-Hermitian systems exhibit four distinct scenarios, dictated by two key factors: the presence of topological order and whether the energy bands cross an EP induced by non-reciprocal hopping.

Disorder-driven EPs and TPTs.—We now examine the effects of random disorder in non-Hermitian systems. Specifically, we introduce static Anderson disorder to the on-site potential energy, with a uniform distribution in the range $[-W/2, W/2]$, where W represents the disorder strength.

We first explore the effects of introducing Anderson

disorder into a clean non-Hermitian system that is topologically trivial and remains before the EP, case ① with redstar shown in Fig. 1(b). As illustrated in Fig. 2(a), as W increases from zero, disorder-averaged $\langle \text{Re}(E_c) \rangle$ and $\langle \text{Re}(E_v) \rangle$ gradually converge and become degenerate beyond a critical point. During this transition, the corresponding imaginary parts, $\langle \text{Im}(E_c) \rangle$ and $\langle \text{Im}(E_v) \rangle$, acquire nonzero conjugate values, as shown in Fig. 2(b), confirming the emergence of an EP. Interestingly, within a certain range of disorder strength, the real parts remain degenerate while the imaginary parts form conjugate pairs, resembling a “PT symmetry-breaking phase” in the subspace. As the disorder strength increases further, $\langle \text{Re}(E_c) \rangle$ and $\langle \text{Re}(E_v) \rangle$ split once more, while $\langle \text{Im}(E_c) \rangle$ and $\langle \text{Im}(E_v) \rangle$ vanish beyond another critical point, signaling the occurrence of a second EP. These two distinct EPs are shown in Fig. 2 (a). Simultaneously, the disorder-averaged spin Bott index $\langle B_s \rangle$ reveals that the system becomes topologically nontrivial upon crossing the second EP, as shown in Fig. 2(c). In the sec. II of the Supplementary Material (SM) [55], we provide the analysis of the s and p band characteristics for E_v and E_c in a random sampler, revealing a band inversion at the second EP, which indicates a TPT that aligns with the spin Bott index results.

We next investigate the effects of Anderson disorder in a clean non-Hermitian system that becomes topologically trivial beyond the EP due to non-reciprocal hopping, case ④ with redstar shown in Fig. 1(c). We find that $\langle \text{Re}(E_c) \rangle$ and $\langle \text{Re}(E_v) \rangle$ remain degenerate within a certain range of disorder strength, while the corresponding imaginary parts, $\langle \text{Im}(E_c) \rangle$ and $\langle \text{Im}(E_v) \rangle$, form complex conjugate pairs, as illustrated in Figs. 2(d) and 2(e). As the disorder strength increases further, $\langle \text{Re}(E_c) \rangle$ and $\langle \text{Re}(E_v) \rangle$ split beyond a critical point, while $\langle \text{Im}(E_c) \rangle$ and $\langle \text{Im}(E_v) \rangle$ vanish, signaling the emergence of an EP. At this EP, the spin Bott index $\langle B_s \rangle$ jumps from zero to one, indicating that the system becomes topologically nontrivial. Although non-reciprocal hopping initially drives the system through an EP and a concurrent TPT (topologically nontrivial to topologically trivial), disorder further induces another transition through both an EP and a TPT (topologically trivial to topologically nontrivial), restoring the system to a topologically nontrivial phase.

In the sec. III of the SM [55], we further explore two additional cases: ② the initial clean non-Hermitian system is topologically trivial beyond an EP, and ③ the system is topologically nontrivial before an EP. In case ②, we also find that disorder drives the system through an EP and a concurrent TPT, but in case ③, as the disorder strength increases, the appearance of the imaginary parts of the energy spectrum indicates that the energy level is broadened, where no clear EP appears. When the disorder is large enough, the system eventually transitions to the trivial phase.

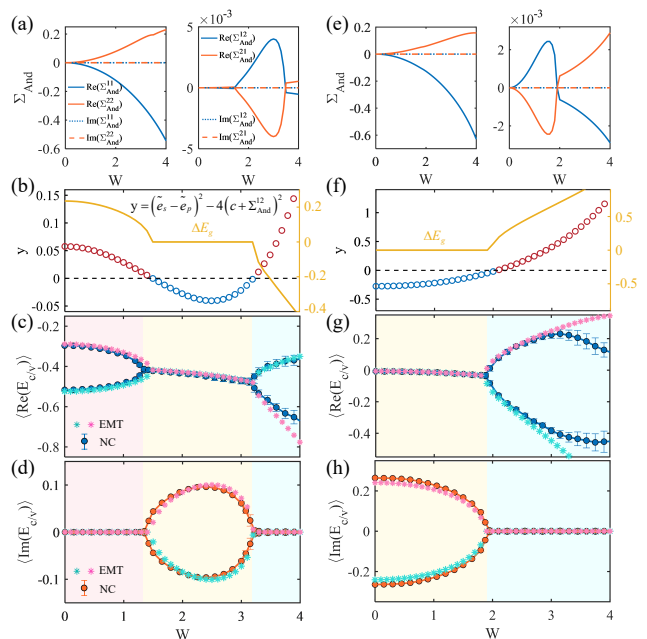


FIG. 3. (a),(e) Elements of the disordered self-energy term Σ_{And}^{ij} as a function of W for $\lambda = 1.2, 2$, respectively. (b),(f) The quantity y (left axis) and energy gap ΔE_g (right axis) as a function of W for $\lambda = 1.2, 2$, respectively. (c),(d),(g),(h) Comparison between EMT and numerical calculations (NC), where (c),(d) correspond to $\lambda = 1.2$ and (g),(h) correspond to $\lambda = 2$.

Effective medium theory.—To understand how disorder induces EPs and TPTs, we employ effective medium theory (EMT). Since the spin-up and spin-down subspaces in Eq. (1) are decoupled, we focus only on the spin-up subspace in the following analysis. EMT introduces a self-energy term to the Hamiltonian to approximate disorder effects, capturing the essential physics [25, 56]. By performing a Fourier transform and folding the energy bands into a two-band model, we derive the spin-up Hamiltonian in momentum space (details can be found in the sec. IV of the SM [55])

$$H_0(\vec{k}) = \begin{pmatrix} H_0^{11} & H_0^{12} \\ H_0^{21} & H_0^{22} \end{pmatrix}, \quad (3)$$

where the detailed expressions for the matrix element H_0^{ij} are provided in the sec. IV of the SM [55].

Within the self-consistent Born approximation [25, 56], the self-energy induced by Anderson disorder is

$$\Sigma_{\text{And}} = \frac{W^2}{48\pi^2} \int_{BZ} d\vec{k} [E + i0^+ - H_0(\vec{k}) - \Sigma_{\text{And}}]^{-1}, \quad (4)$$

where the integral is over the first Brillouin zone. After self-consistently solving Eq. (4), the numerical results of self-energy for cases ① and ④ are presented in Figs. 3(a) and 3(e). Note that the imaginary parts of

the self-energy terms remain negligible small, indicating the absence of energy level broadening within the studied disorder strength range. This is consistent with the numerical results obtained in Fig. 2, where the fluctuations in energy levels, represented by the error bars, are minimal. Additionally, we note that the off-diagonal terms satisfy $\Sigma_{\text{And}}^{12} = -\Sigma_{\text{And}}^{21}$.

Then we diagonalize the effective medium Hamiltonian $H_{\text{EMH}} = H_0 + \Sigma_{\text{And}}$ at the Γ point to obtain the disorder averaged conduction and valence eigenvalues

$$\langle E_{c/v} \rangle = \frac{\tilde{e}_s + \tilde{e}_p \pm \sqrt{(\tilde{e}_s - \tilde{e}_p)^2 - 4(c + \Sigma_{\text{And}}^{12})^2}}{2}, \quad (5)$$

where $\tilde{e}_s = \varepsilon_s + 2V_{ss\sigma}(1 + 3\cosh(\kappa)) + \Sigma_{\text{And}}^{11}$, $\tilde{e}_p = \varepsilon_p + (V_{pp\sigma} + V_{pp\pi})(1 + 3\cosh(\kappa)) + \lambda + \Sigma_{\text{And}}^{22}$, and $c = \frac{3\sqrt{6}+2\sqrt{2}}{3}V_{sp\sigma}\sinh(\kappa)$. To begin our analysis, we first examine the clean case by setting $\Sigma_{\text{And}} = 0$. We find that the conduction and valence energy levels can pass through an EP once as κ reaches critical point dominated by $(\tilde{e}_s - \tilde{e}_p)^2 - 4c^2 = 0$ where the band gap $\Delta E_g = \text{Re}(E_c - E_v)$ equals to zero. Note that the TPT occurs simultaneously with the EP when the Hermitian system exhibits an inverted band gap, i.e., $\tilde{e}_s < \tilde{e}_p$, as shown in Fig. 1(c).

In the following, we demonstrate how random disorder induce EPs and concurrent TPTs based on EMT. We begin by analyzing case ①, where $(\tilde{e}_s - \tilde{e}_p)^2 - 4c^2 > 0$ and $\tilde{e}_s > \tilde{e}_p$ in the clean limit. As shown in Fig. 3(a), the diagonal self-energy term Σ_{And}^{22} is positive, raising the valance band \tilde{e}_p , while Σ_{And}^{11} is negative, lowering the conduction band \tilde{e}_s as disorder strength increases. To track the evolution of the eigenvalues with disorder, we define the quantity $y = (\tilde{e}_s - \tilde{e}_p)^2 - 4(c + \Sigma_{\text{And}}^{12})^2$ which appears under the square root in Eq. (5), as shown in Fig. 3(b). In addition to the diagonal terms of the self-energy renormalizing the energy levels \tilde{e}_s and \tilde{e}_p , the off-diagonal term Σ_{And}^{12} emerges. Although its magnitude is minor compared to the non-reciprocal hopping in Fig. 3(a), it nominally contributes to inter-orbital $s - p$ coupling. As the disorder strength increases from zero, y decreases from a positive value. Once y reaches zero, $\langle E_c \rangle$ and $\langle E_v \rangle$ become degenerate, and the Hamiltonian H_{EMH} becomes defective, signaling the first EP. With further increase in disorder strength, y becomes negative, leading to complex-conjugate eigenvalues with degenerate real parts. Upon reaching a minimum, y reverses direction and returns to zero, marking the second EP. Beyond this point, $y > 0$ and eigenvalues become purely real again, completing the real-complex-real transition. Simultaneously, a band inversion occurs at the second EP, as indicated by ΔE_g in Fig. 3(b), indicating a concurrent TPT. The non-monotonic behavior of y reflects the intricate interplay between disorder-induced energy level renormalization and non-reciprocal hopping-driven inter-level coupling. Importantly, EMT without any ad-

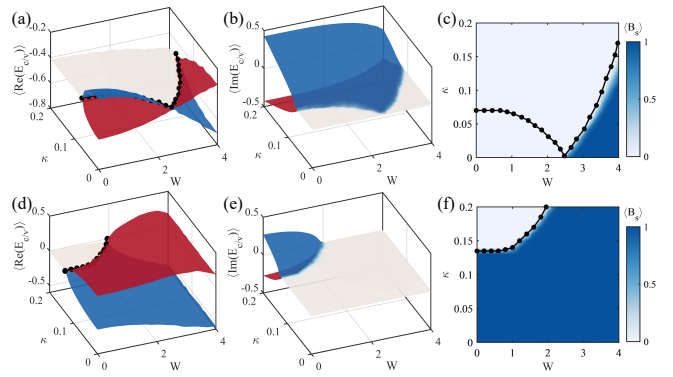


FIG. 4. Phase diagram of disorder-averaged $\langle \text{Re}(E_{c/v}) \rangle$, $\langle \text{Im}(E_{c/v}) \rangle$ and $\langle B_s \rangle$ in the parameter space of κ and σ . (a)-(c) correspond to case ①, while (d)-(f) correspond to case ④. Each data point is averaged over 100 disorder realizations. Black dotted lines indicate the EP lines. The system size is 20×20 with periodic boundary conditions.

justable parameters, accurately captures the emergence of both EPs and the associated TPT, in excellent agreement with real-space numerical calculations shown in Figs. 3(c) and 3(d).

Unlike case ①, in case ④, where $(\tilde{e}_s - \tilde{e}_p)^2 - 4c^2 < 0$ and $\tilde{e}_s < \tilde{e}_p$ in the clean limit, the signs of the diagonal terms are the same as in the previous case ①, but in this case there is no band inversion as the disorder increases. The evolution of the quantity y is presented in Fig. 3(f). Initially, y starts from a negative value and increases up to zero due to the disorder effects. When y crosses zero, an EP emerges. As y continues to increase and becomes positive, $\langle E_c \rangle$ and $\langle E_v \rangle$ become pure real values again, leading to the reopening of a real gap, as indicated by ΔE_g in Fig. 3(f). This confirms that the TPT occurs at the EP. Similarly, Figs. 3(g) and 3(h) show the strong agreement between the EMT and numerical calculations.

Phase diagram.—Finally, we present the disorder-averaged $\langle \text{Re}(E_{c/v}) \rangle$, $\langle \text{Im}(E_{c/v}) \rangle$ and $\langle B_s \rangle$ in the parameter space of κ and W . In case ①, two EP lines (black dotted lines) emerge from the TPT point of Hermitian case at $\kappa = 0, W = 2.5$ (see sec. V in the SM). As κ increases, two EP lines separate, with one shifting toward smaller W and the other, which coincides with the TPT, extending toward larger values as shown in Fig. 4(c). In contrast, case ④ exhibits only a single EP line concurrent with TPTs, as shown in Figs. 4(d)-4(f). Therefore, the disorder-induced EPs and TPTs represent a robust phenomenon, persisting over a broad parameter range and not confined to fine-tuned conditions.

Conclusion.—In conclusion, we have shown that random disorder can induce EPs in non-Hermitian systems. Depending on the nature of the clean non-Hermitian system, disorder-induced EPs can either coincide with TPTs or not. The mechanism underlying these disorder-induced EPs and concurrent TPTs is applicable to a

broad range of parameters. We anticipate a significant extension of EPs from the clean system to disordered non-Hermitian systems. Our results reveal the intricate interplay between disorder, non-Hermiticity, and topology, offering new avenues for investigating novel physical phenomena driven by disorder-induced EPs and concurrent TPTs.

This work is supported by the National Natural Science Foundation of China (Grant No. 12474047, 12174231), the Fund for Shanxi “1331 Project”, Research Project Supported by Shanxi Scholarship Council of China. This research was partially conducted using the High Performance Computer of Shanxi University.

*)zhanglei@sxu.edu.cn

†)chenjun@sxu.edu.cn

-
- [1] C. M. Bender and S. Boettcher, Real spectra in non-Hermitian Hamiltonians having PT symmetry, *Phys. Rev. Lett.* **80**, 5243 (1998).
- [2] W. Heiss, Exceptional points of non-Hermitian operators, *J. Phys. Math. Gen.* **37**, 2455 (2004).
- [3] C. E. Rüter, K. G. Makris, R. El-Ganainy, D. N. Christodoulides, M. Segev, and D. Kip, Observation of parity–time symmetry in optics, *Nat. Phys.* **6**, 192 (2010).
- [4] A. Regensburger, C. Bersch, M.-A. Miri, G. Onishchukov, D. N. Christodoulides, and U. Peschel, Parity–time synthetic photonic lattices, *Nature* **488**, 167 (2012).
- [5] B. Zhen, C. W. Hsu, Y. Igarashi, L. Lu, I. Kaminer, A. Pick, S.-L. Chua, J. D. Joannopoulos, and M. Soljačić, Spawning rings of exceptional points out of Dirac cones, *Nature* **525**, 354 (2015).
- [6] L. Feng, R. El-Ganainy, and L. Ge, Non-Hermitian photonics based on parity–time symmetry, *Nat. Photonics* **11**, 752 (2017).
- [7] M.-A. Miri and A. Alu, Exceptional points in optics and photonics, *Science* **363**, eaar7709 (2019).
- [8] A. Guo, G. J. Salamo, D. Duchesne, R. Morandotti, M. Volatier-Ravat, V. Aimez, G. A. Siviloglou, and D. N. Christodoulides, Observation of PT-symmetry breaking in complex optical potentials, *Phys. Rev. Lett.* **103**, 093902 (2009).
- [9] X.-Y. Lü, H. Jing, J.-Y. Ma, and Y. Wu, PT-symmetry-breaking chaos in optomechanics, *Phys. Rev. Lett.* **114**, 253601 (2015).
- [10] Z. Gong, Y. Ashida, K. Kawabata, K. Takasan, S. Higashikawa, and M. Ueda, Topological phases of non-Hermitian systems, *Phys. Rev. X* **8**, 031079 (2018).
- [11] H. Shen, B. Zhen, and L. Fu, Topological band theory for non-Hermitian Hamiltonians, *Phys. Rev. Lett.* **120**, 146402 (2018).
- [12] S. Yao and Z. Wang, Edge states and topological invariants of non-Hermitian systems, *Phys. Rev. Lett.* **121**, 086803 (2018).
- [13] F. Song, S. Yao, and Z. Wang, Non-Hermitian topological invariants in real space, *Phys. Rev. Lett.* **123**, 246801 (2019).
- [14] K. Kawabata, K. Shiozaki, M. Ueda, and M. Sato, Symmetry and topology in non-Hermitian physics, *Phys. Rev. X* **9**, 041015 (2019).
- [15] E. J. Bergholtz, J. C. Budich, and F. K. Kunst, Exceptional topology of non-Hermitian systems, *Rev. Mod. Phys.* **93**, 015005 (2021).
- [16] K. Ding, C. Fang, and G. Ma, Non-Hermitian topology and exceptional-point geometries, *Nat. Rev. Phys.* **4**, 745 (2022).
- [17] N. Okuma and M. Sato, Non-Hermitian topological phenomena: A review, *Annu. Rev. Condens. Matter Phys.* **14**, 83 (2023).
- [18] L. Li, C. H. Lee, S. Mu, and J. Gong, Critical non-Hermitian skin effect, *Nat. Commun.* **11**, 5491 (2020).
- [19] X. Zhang, Y. Tian, J.-H. Jiang, M.-H. Lu, and Y.-F. Chen, Observation of higher-order non-Hermitian skin effect, *Nat. Commun.* **12**, 5377 (2021).
- [20] S. Liu, R. Shao, S. Ma, L. Zhang, O. You, H. Wu, Y. J. Xiang, T. J. Cui, and S. Zhang, Non-Hermitian skin effect in a non-Hermitian electrical circuit, *Research* **2021**, 5608038 (2021).
- [21] D. Zou, T. Chen, W. He, J. Bao, C. H. Lee, H. Sun, and X. Zhang, Observation of hybrid higher-order skin-topological effect in non-Hermitian topoelectrical circuits, *Nat. Commun.* **12**, 7201 (2021).
- [22] R. Lin, T. Tai, L. Li, and C. H. Lee, Topological non-Hermitian skin effect, *Front. Phys.* **18**, 53605 (2023).
- [23] K. Kawabata, T. Numasawa, and S. Ryu, Entanglement phase transition induced by the non-Hermitian skin effect, *Phys. Rev. X* **13**, 021007 (2023).
- [24] J. Li, R.-L. Chu, J. K. Jain, and S.-Q. Shen, Topological Anderson insulator, *Phys. Rev. Lett.* **102**, 136806 (2009).
- [25] C. W. Groth, M. Wimmer, A. R. Akhmerov, J. Tworzydło, and C. W. J. Beenakker, Theory of the topological Anderson insulator, *Phys. Rev. Lett.* **103**, 196805 (2009).
- [26] H.-M. Guo, G. Rosenberg, G. Refael, and M. Franz, Topological Anderson insulator in three dimensions, *Phys. Rev. Lett.* **105**, 216601 (2010).
- [27] C. Liu, W. Gao, B. Yang, and S. Zhang, Disorder-induced topological state transition in photonic metamaterials, *Phys. Rev. Lett.* **119**, 183901 (2017).
- [28] C.-A. Li, B. Fu, Z.-A. Hu, J. Li, and S.-Q. Shen, Topological phase transitions in disordered electric quadrupole insulators, *Phys. Rev. Lett.* **125**, 166801 (2020).
- [29] S. Stützer, Y. Plotnik, Y. Lumer, P. Titum, N. H. Lindner, M. Segev, M. C. Rechtsman, and A. Szameit, Photonic topological Anderson insulators, *Nature* **560**, 461 (2018).
- [30] E. J. Meier, F. A. An, A. Dauphin, M. Maffei, P. Massignan, T. L. Hughes, and B. Gadway, Observation of the topological Anderson insulator in disordered atomic wires, *Science* **362**, 929 (2018).
- [31] X. Cui, R.-Y. Zhang, Z.-Q. Zhang, and C. T. Chan, Photonic Z_2 topological Anderson insulators, *Phys. Rev. Lett.* **129**, 043902 (2022).
- [32] X.-D. Chen, Z.-X. Gao, X. Cui, H.-C. Mo, W.-J. Chen, R.-Y. Zhang, C. Chan, and J.-W. Dong, Realization of time-reversal invariant photonic topological Anderson insulators, *Phys. Rev. Lett.* **133**, 133802 (2024).
- [33] Z.-Q. Zhang, B.-L. Wu, J. Song, and H. Jiang, Topological Anderson insulator in electric circuits, *Phys. Rev. B* **100**, 184202 (2019).
- [34] D.-W. Zhang, L.-Z. Tang, L.-J. Lang, H. Yan, and S.-L. Zhu, Non-Hermitian topological Anderson insulators,

- Sci. China-Phys. Mech. Astron. **63**, 267062 (2020).
- [35] Z. Gu, H. Gao, H. Xue, D. Wang, J. Guo, Z. Su, B. Zhang, and J. Zhu, Observation of an acoustic non-Hermitian topological Anderson insulator, *Sci. China-Phys. Mech. Astron* **66**, 294311 (2023).
- [36] W. Zhang, D. Zou, Q. Pei, W. He, J. Bao, H. Sun, and X. Zhang, Experimental observation of higher-order topological Anderson insulators, *Phys. Rev. Lett.* **126**, 146802 (2021).
- [37] Q. Lin, T. Li, L. Xiao, K. Wang, W. Yi, and P. Xue, Observation of non-Hermitian topological Anderson insulator in quantum dynamics, *Nat. Commun.* **13**, 3229 (2022).
- [38] R. Chen, D.-H. Xu, and B. Zhou, Disorder-induced topological phase transitions on Lieb lattices, *Phys. Rev. B* **96**, 205304 (2017).
- [39] A. Agarwala and V. B. Shenoy, Topological insulators in amorphous systems, *Phys. Rev. Lett.* **118**, 236402 (2017).
- [40] N. P. Mitchell, L. M. Nash, D. Hexner, A. M. Turner, and W. T. Irvine, Amorphous topological insulators constructed from random point sets, *Nat. Phys.* **14**, 380 (2018).
- [41] K. Pöyhönen, I. Sahlberg, A. Westström, and T. Ojanen, Amorphous topological superconductivity in a Shiba glass, *Nat. Commun.* **9**, 2103 (2018).
- [42] Y.-B. Yang, T. Qin, D.-L. Deng, L.-M. Duan, and Y. Xu, Topological amorphous metals, *Phys. Rev. Lett.* **123**, 076401 (2019).
- [43] C. Wang, T. Cheng, Z. Liu, F. Liu, and H. Huang, Structural amorphization-induced topological order, *Phys. Rev. Lett.* **128**, 056401 (2022).
- [44] X. Cheng, T. Qu, L. Xiao, S. Jia, J. Chen, and L. Zhang, Topological Anderson amorphous insulator, *Phys. Rev. B* **108**, L081110 (2023).
- [45] P. Zhou, G.-G. Liu, X. Ren, Y. Yang, H. Xue, L. Bi, L. Deng, Y. Chong, and B. Zhang, Photonic amorphous topological insulator, *Light Sci. Appl.* **9**, 133 (2020).
- [46] J.-H. Wang, Y.-B. Yang, N. Dai, and Y. Xu, Structural-disorder-induced second-order topological insulators in three dimensions, *Phys. Rev. Lett.* **126**, 206404 (2021).
- [47] P. Corbae, S. Ciocys, D. Varjas, E. Kennedy, S. Zeltmann, M. Molina-Ruiz, S. M. Griffin, C. Jozwiak, Z. Chen, L.-W. Wang, A. M. Minor, M. Scott, A. G. Grushin, A. Lanzara, and F. Hellman, Observation of spin-momentum locked surface states in amorphous Bi_2Se_3 , *Nat. Mater.* **22**, 200 (2023).
- [48] Z. Zhang, P. Delplace, and R. Fleury, Anomalous topological waves in strongly amorphous scattering networks, *Sci. Adv.* **9**, eadg3186 (2023).
- [49] T. Qu, M. Wang, X. Cheng, X. Cui, R.-Y. Zhang, Z.-Q. Zhang, L. Zhang, J. Chen, and C. Chan, Topological photonic alloy, *Phys. Rev. Lett.* **132**, 223802 (2024).
- [50] M. Papaj, H. Isobe, and L. Fu, Nodal arc of disordered Dirac fermions and non-Hermitian band theory, *Phys. Rev. B* **99**, 201107 (2019).
- [51] A. A. Zyuzin and P. Simon, Disorder-induced exceptional points and nodal lines in Dirac superconductors, *Phys. Rev. B* **99**, 165145 (2019).
- [52] Z. Wang, K.-H. Jin, and F. Liu, Quantum spin Hall phase in 2D trigonal lattice, *Nat. Commun.* **7**, 12746 (2016).
- [53] H. Huang and F. Liu, Quantum spin Hall effect and spin Bott index in a quasicrystal lattice, *Phys. Rev. Lett.* **121**, 126401 (2018).
- [54] J. C. Slater and G. F. Koster, Simplified LCAO method for the periodic potential problem, *Phys. Rev.* **94**, 1498 (1954).
- [55] See Supplemental Material at <http://link.aps.org/supplemental/XXX> for (I) spin Bott index in Hermitian and non-Hermitian systems, (II) orbital-resolved band characteristics in disordered system, (III) two additional cases, (IV) effective medium theory and (V) disorder-driven topological phase transitions in Hermitian system, which includes Refs. [25, 43, 44, 53, 56–59].
- [56] P. Sheng, *Introduction to wave scattering, localization and mesoscopic phenomena*. (Springer, Berlin, Heidelberg, 2006).
- [57] D. Toniolo, Time-dependent topological systems: A study of the Bott index, *Phys. Rev. B* **98**, 235425 (2018).
- [58] H. Huang and F. Liu, Theory of spin Bott index for quantum spin Hall states in nonperiodic systems, *Phys. Rev. B* **98**, 125130 (2018).
- [59] S. Manna and B. Roy, Inner skin effects on non-Hermitian topological fractals, *Commun. Phys.* **6**, 10 (2023).